

Kinetics of Transformation of Al_2O_3 to $\text{MgO}\cdot\text{Al}_2\text{O}_3$ Spinel Inclusions in Mg-Containing Steel



CHUNYANG LIU, MOTOKI YAGI, XU GAO, SUN-JOONG KIM, FUXIANG HUANG, SHIGERU UEDA, and SHIN-YA KITAMURA

During ladle furnace refining, initial Al_2O_3 inclusions generally transform into $\text{MgO}\cdot\text{Al}_2\text{O}_3$ spinel inclusions; these generated spinel inclusions consequently deteriorate the product quality. In this study, the transformation from Al_2O_3 to $\text{MgO}\cdot\text{Al}_2\text{O}_3$ was investigated by immersing an Al_2O_3 rod into molten steel, which was in equilibrium with both MgO and $\text{MgO}\cdot\text{Al}_2\text{O}_3$ spinel-saturated slag. A spinel layer, with a thickness of 4 μm , was generated on the Al_2O_3 rod surface just 10 s after its immersion at 1873 K (1600 °C). The thickness of the formed spinel layer increased with the immersion period and temperature. Moreover, the MgO content of the generated spinel layer also increased with the immersion period. In this study, the chemical reaction rate at 1873 K (1600 °C) was assumed to be sufficiently high, and only diffusion was considered as a rate-controlling step for this transformation. By evaluating the activation energy, MgO diffusion in the generated spinel layer was found to be the rate-controlling step. In addition, this estimation was confirmed by observing the Mg and Al concentration gradients in the generated spinel layer. The results of this study suggest that the MgO diffusion in the spinel inclusions plays a substantial role with regard to their formation kinetics.

DOI: 10.1007/s11663-017-1122-6

© The Minerals, Metals & Materials Society and ASM International 2017

I. INTRODUCTION

INCLUSIONS play a crucial role in determining steel quality because their properties, such as their plasticity and thermal expansion, differ to those of the steel matrix; they then act as stress raisers and a source of cracks. In general, inclusions are harmful, except in certain circumstances, where inclusions with extremely small sizes can be utilized as nucleation sites for phase transformation. In many cases, during ladle furnace (LF) refining, Al_2O_3 inclusions, a common deoxidation product, often degrade into $\text{MgO}\cdot\text{Al}_2\text{O}_3$ spinel inclusions (for simplicity, denoted as spinel in this paper).

This spinel is generally considered harmful because many studies have shown that steel surface deterioration or impaired fatigue resistance is often related to spinel. In addition, spinel can easily sinter with the nozzle material and disturb the casting process. Therefore, the control of spinel generation is currently attracting worldwide research attention.^[1–25]

Many studies have been conducted to clarify the spinel generation mechanism. To simplify, spinel inclusions can form in two ways: In the first case, the inclusions are caused by entrapped slag droplets or ladle glaze; these inclusions are known as ‘exogenous’ inclusions.^[1,2] In the other case, the inclusions are caused by interaction between the steel melt and Al_2O_3 inclusions; these inclusions are known as ‘endogenous’ inclusions.^[3,4] Park *et al.*^[1] found that following interaction with the Al in the steel melt, a $\text{MgO}\cdot\text{Al}_2\text{O}_3$ phase precipitated in the entrapped $\text{CaO}\cdot\text{MgO}\cdot\text{Al}_2\text{O}_3\cdot\text{SiO}_2$ slag droplets. They considered that this precipitated spinel phase could separate from the slag droplets and form inclusions. Son *et al.*^[2] studied the reactions between glazed refractory and Al-deoxidized molten steel. They found that the refining slag that adhered onto the surface of the refractory (ladle glaze) separated into spinel and a $\text{CaO}\cdot\text{Al}_2\text{O}_3$ phase during cooling. They considered that the ladle glaze became entrapped in the steel melt and formed spinel and $\text{CaO}\cdot\text{Al}_2\text{O}_3$ -type inclusions. In general, the spinel inclusions that are generated through the exogenous process

CHUNYANG LIU is with the Department of Metallurgy, Graduate School of Engineering, Tohoku University, 2-1-1 Katahira, Aoba-ku, Sendai 980-8577, Japan. Contact e-mail: chunyangliu@163.com
MOTOKI YAGI is with the Central Japan Railway, 1-1-4 Meieki, Nakamura-ku, Nagoya, Aichi 450-6101 Japan. XU GAO, SHIGERU UEDA, and SHIN-YA KITAMURA are with the Institute of Multi-disciplinary Research for Advanced Materials, Tohoku University, 2-1-1 Katahira, Aoba-ku, Sendai, 980-8577 Japan. SUN-JOONG KIM is with the Department of Materials Science & Engineering, College of Engineering, Chosun University, 309, Pilmun-daero, Dong-gu, Gwangju 61452, Korea. FUXIANG HUANG is with the School of Metallurgical and Ecological Engineering, University of Science and Technology Beijing, 30 Xueyuan Road, Haidian District, Beijing City 100083, P.R.China.

Manuscript submitted February 23, 2017.

Article published online November 6, 2017.

simultaneously exist with CaO-Al₂O₃-type or CaO-SiO₂-type inclusions. However, in actual production, only spinel and Al₂O₃ inclusions were detected several minutes after Al deoxidation; therefore, the spinel was not predominantly generated *via* an exogenous mechanism. Moreover, Harada *et al.*^[3] summarized the spinel generation mechanism that occurs *via* the endogenous process, as shown in the following three reactions; they concluded that Reaction [3] was thermodynamically favorable.



However, in an actual refining process, MgO inclusions are normally not observed in the steel melt prior to Al addition.^[5] Thermodynamically, under steelmaking conditions, Reactions [1] and [2] could both occur and generate spinel inclusions; however, one of the authors of this paper^[4] concluded that the Al₂O₃ transformation (Reaction [2]) was the preferential spinel generation route on the basis of kinetic experiments. In addition, Wang *et al.*^[5] also found that during LF refining, only Al₂O₃ inclusions were observed just following Al deoxidation; the number of Al₂O₃ inclusions decreased dramatically, while that of the spinel subsequently increased sharply. In their research, the increase in the mass ratio of spinel inclusions and the reduction in Al₂O₃ inclusions precisely correlated with the results of Reaction [2]. Therefore, they concluded that the transformation of Al₂O₃ was the predominant mechanism for spinel generation.

In practice, spinel inclusions are inevitably generated regardless of the generation mechanism. The spinel generation process consists of two steps. In the first step, Mg is supplied from MgO sources to the steel melt. This is followed by the second and final step, which is the transformation of the Al₂O₃ inclusions. Therefore, the kinetics of both the Mg supply and Al₂O₃ transformation should be studied to determine control measures. The rate-controlling step was determined in terms of the kinetics. Okuyama *et al.*^[6] investigated the variation in the Mg content of steel that was reacted with slag using an induction furnace. Based on theoretical analysis of the experimental results, they concluded that the Mg transfer in the steel melt functioned as the rate-controlling step for the Mg supply. Harada *et al.*^[3] studied the rate of supply of Mg to molten steel from MgO refractory; this was performed by immersing and rotating a cylinder of sintered MgO in a steel melt. They also concluded that the Mg transfer in the steel melt functioned as the rate-controlling step for the Mg supply. One of the authors of the current study^[7] investigated the dissolution of Mg from MgO refractory, MgO-C refractory, and MgO-containing slag to Al-killed steel. Their experimental results correlated with a model calculation, which assumed that the Mg transfer in the steel melt functioned as the rate-controlling step for the Mg supply. From the

above works, it is widely accepted that Mg transfer in a steel melt functions as the rate-controlling step for Mg supply, regardless of the MgO source. With regard to the second step of spinel generation, Al₂O₃ inclusion transformation, few studies have been conducted. In previous works,^[6,7] such inclusions were assumed to be in equilibrium with the steel melt. However, one of the authors of the current study^[4] observed that spinel inclusions had cores with low MgO contents (MgO 25 pct-Al₂O₃ 75 pct) and outer layers with high MgO contents (MgO 41 pct-Al₂O₃ 59 pct) following Al₂O₃ inclusion transformation; these results were based on an experiment that used MgO-C refractory as a MgO source. These results indicated that a MgO gradient existed inside the solid inclusions, which contradicted the assumption that the inclusions were in equilibrium with the steel melt. Therefore, in terms of precise inclusion control, the kinetics for the spinel generation shall be studied. In detail, it is necessary to determine the rate-controlling step associated with the Al₂O₃ transformation to spinel and clarify the transformation rate.

In this study, to investigate the rate of transformation of Al₂O₃ to spinel, an Al₂O₃ rod was immersed into Mg-containing molten steel, and the rate of formation of the spinel layer on the surface of the Al₂O₃ rod was measured. Although Al₂O₃ inclusions are small and usually consist of a single crystal, a polycrystalline Al₂O₃ rod of macroscopic size was selected to measure the transformation rate. In addition, prior to the immersion of the Al₂O₃ rod, the Mg-containing steel was equilibrated with slag that was saturated with both MgO and MgO-saturated spinel, and thus the transformation rate was studied exclusively without the influence of the Mg supply rate.

II. EXPERIMENTAL METHOD

A. Raw Materials

The slag employed in this study was composed of 25 mass pct CaO-20 mass pct MgO-55 mass pct Al₂O₃ (all the compositions in this paper are given in mass percentage, unless specifically stated). A diagram showing the projection of the slag composition on the CaO-MgO-Al₂O₃ system is shown in Figure 1. Therefore, the liquid phase of the slag employed was saturated with both MgO and MgO-saturated MgO·Al₂O₃. To prepare the slag, CaO was prepared by heating CaCO₃ at 1273 K (1000 °C) for 12 hours, which was subsequently mixed with reagent grade MgO and Al₂O₃. Subsequently, the mixture was pressed into tablets and sintered at 1473 K (1200 °C) for 12 hours; it then solidified and formed lump slag.

A metal with a composition of Fe-11 pct Cr-0.25 pct Al was used in this study. To prepare this metal, electrolytic Fe together with high-purity Cr (99.9 pct) and Al (99.999 pct) metals were melted in an argon arc furnace to produce the master steel.

Dense Al₂O₃ rods (density: 3.9 g/cm³) were cut from an α-Al₂O₃ (99.6 pct) thermocouple protective tube with an outer diameter of 6 mm.

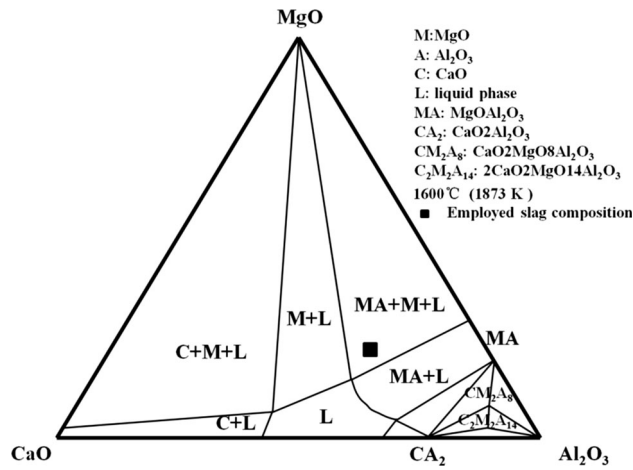


Fig. 1—Projection of the employed slag composition on the CaO-MgO-Al₂O₃ phase diagram.

B. Experimental Procedure

The experimental set-up for this research is shown in Figure 2. The experiment was conducted using an induction furnace (195 kHz). Prior to heating, 150 g of the prepared metal, together with 13 g of the lump slag, was loaded into a dense MgO crucible (ID: 32 mm, OD: 38 mm, H: 100 mm). Subsequently, the chamber of the furnace was subjected to vacuum conditions, and then purged with purified argon. This process was repeated three times. To achieve purification, the argon (99.9999 pct) was passed through heated Mg chips [573 K (300 °C)] to remove oxygen (< 0.1 ppm); it then flowed into the chamber of the furnace. Subsequently, the metal was heated to 1873 K (1600 °C), and the temperature of the molten steel was measured by immersing a thermocouple protected by an MgO tube into the melt. Subsequently, the system was maintained at 1873 K (1600 °C) for 2 hours for the melt to attain both MgO and spinel saturation. Then, the pre-heated Al₂O₃ rod was immersed into the molten steel, and this time was considered the starting point of the experiment. Prior to immersion, the Al₂O₃ rod was positioned just above the surface of the slag, and pre-heated for 4 hours. Following its immersion for a pre-determined time, the Al₂O₃ rod was removed and air-cooled, while the molten steel together with the crucible was rapidly quenched with water. The Al₂O₃ rod was immersed for 0, 10, 20, 30, 60, or 180 seconds, respectively. To clarify the influence of temperature, experiments were also conducted at 1823 K (1550 °C) and 1923 K (1650 °C). In these cases, the steel was allowed to react with the slag at 1873 K (1600 °C) for 1 hour 40 minutes, and subsequently, the temperature was altered to the target value within 20 minutes.

C. Analysis

Following quenching, the center portion of the metal (5 mm above the base) was cut for both chemical composition analysis and inclusion observation. For the chemical analysis, the Al and Mg contents were analyzed using inductively coupled plasma atomic emission

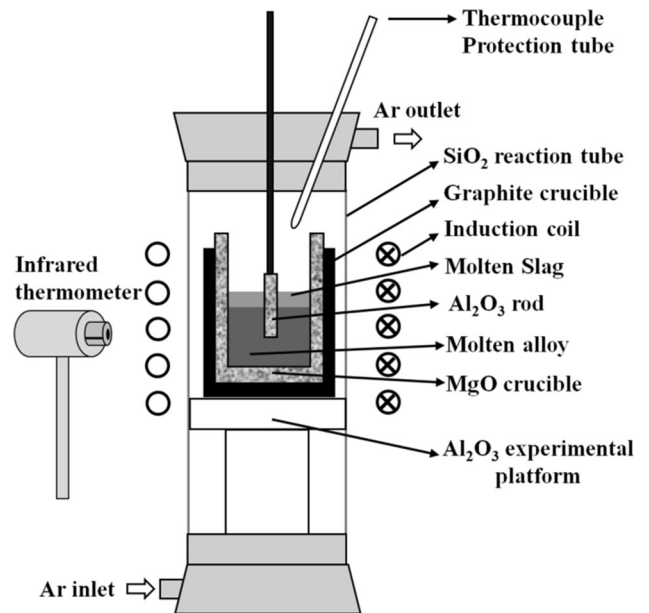


Fig. 2—Schematic of experimental apparatus.

spectroscopy (ICP-AES). The lower limit of quantitation of ICP analysis method in this study has been confirmed to be much lower than the analyzed values shown in the following figures, and thus the analysis accuracy of Mg is considered to be reliable. The Total Oxygen (T.O) of the steel sample was measured by the infrared X-ray absorption method. For inclusion observation, a scanning electron microscope (SEM) equipped with an automatic inclusion analysis system was used (P-SEM, ASPEX corporation). For the P-SEM observation, the accelerating voltage used for EDS analysis of inclusions was 15 kv. During the P-SEM analysis, Mg, Al, Fe, Ca, O, S, and Cr were selected as target elements since they existed in the molten steel sample. The inclusions were assumed to consist of MgO, Al₂O₃, and CaO, and the analyzed values of Mg, Al, and Ca were converted to oxide values using a stoichiometric relationship. The values of Fe and Cr were ignored as it was assumed that they were caused by the analysis of the metal phase. The value of S was also ignored because of its low concentration. It should be noted that during the P-SEM observation, inclusions with sizes smaller than 1 μm were not detected, and the scan area for each sample was greater than 30 mm². To observe the growth of the spinel layer on the Al₂O₃ rod, the cooled Al₂O₃ rod was embedded in resin and cut; the cross section was then polished and observed using an electron probe micro-analyzer (EPMA). For the EPMA analysis, the accelerating voltage was 15 kv and WDS was used.

III. EXPERIMENTAL RESULTS

A. Transformation of Al₂O₃ to spinel at 1873 K (1600 °C)

The change in the metal composition (Al, Mg, T.O) is shown in Figure 3. It should be noted that the composition at 0 minute was analyzed using the quenched

metal, which was equilibrated with slag for 2 hours without immersion of the Al_2O_3 rod. As shown in Figure 3, over the period of 0 to 180 seconds, the Al content slightly increased, while the Mg content slightly decreased. Under the current experimental conditions, the Al and Mg contents of the metal should change *via* the following chemical reaction:



Therefore, the reduction in the molar amount of Mg should be 1.5 times that of the increase in Al. However, the current results showed that the Al content of the metal melt increased by approximately 120 ppm, while the Mg content only decreased by several ppm. This deviation would be caused by the continuous supply of Mg from the slag. Therefore, the Mg content of the molten metal was considered to be determined by the kinetic balance of the consumption due to the spinel generation and the supply from the slag. However, the overall Mg concentration decreased, which indicated that the rate of supply of Mg from the slag was insufficient to compensate for the Mg consumption *via* Reaction [4]. In addition, the T.O content should be constant because the slag and metal react for 2 hours prior to the Al_2O_3 rod immersion, and the steel melt composition is always in the region of the MgO-saturated spinel. However, it fluctuated within 3 ppm, which could be caused by a measurement error.

The element mapping images of O, Ca, Al, and Mg near the surface of the Al_2O_3 rod, following its immersion for 10 and 60 seconds, are shown in Figure 4. In these element mapping images, the highest and lowest O contents are 50 and 0 pct, respectively. The respective contents are 10 and 0 pct for Ca; 70 and 0 pct for Al; and 16 and 0 pct for Mg. On the surface of the Al_2O_3 rod, an Mg-enriched area with Al depletion was observed. The results of the quantitative analysis of this Mg-enriched area are also summarized in Figure 4. For spinel, according to the Al_2O_3 -MgO binary phase diagram, the mass ratio of MgO and Al_2O_3 should be in

the range of 0.234 to 0.408^[26]; therefore, the MgO-enriched area was considered as spinel (alumina-saturated spinel at 10 seconds). In addition, the CaO content of the MgO-enriched area was negligible, which indicated that no reaction between the Al_2O_3 rod and slag occurred because the rod was rapidly removed following the given immersion time and there was a short period of contact between the rod surface and slag. The thickness of the spinel layer was measured using the magnified EPMA images. The change in the thickness of the formed spinel layer as a function of time is shown in Figure 5. The spinel layer thickness changed with position and 10 positions were analyzed for each sample and in Figure 5, the data were presented with an error bar. A spinel layer, with a thickness of 4 μm , generated on the Al_2O_3 rod surface after immersion for only 10 seconds. Then, the thickness of the layer increased continuously with extended immersion time. This increment followed a parabolic law which indicated that diffusion could be the rate-controlling step, and this will be discussed in detail later. In addition, the thickness at 180 seconds immersion period was not shown in this figure because the thickness was very thin (even thinner than that at 60 s immersion period), and it was considered that the grown spinel layer would detach from the Al_2O_3 rod.

The line scan of the spinel layer on the Al_2O_3 rod surface, which formed following 30 seconds of immersion at 1873 K (1600 °C), is shown in Figure 6. The horizontal axis indicated the position and the vertical axis indicated the observed elemental intensity. In the spinel phase, the Al content gradually decreased from the interface of the Al_2O_3 rod and spinel to the surface (interface of spinel and molten steel); however, the respective Mg content increased. Line scans of the generated spinel layer, with both short and long immersion periods, were conducted; the Mg and Al gradients were observed for each immersion period. To observe the variation in the composition of the spinel layer with the immersion period, the MgO content of the center portion of the spinel layer was used to represent the average composition; its variation as a function of time is shown in Figure 7. Initially, the composition of the layer was close to that of the Al_2O_3 -saturated spinel; following 30 seconds, it entered into the stable zone of the spinel.

Using P-SEM analysis, the composition of the inclusions was confirmed as the binary system of Al_2O_3 and MgO, because CaO was not detected in any of the inclusions. The variation in the MgO content of the inclusions in the steel is shown in Figure 8 as a function of time. The steel had already reached equilibrium with the slag saturated with the MgO and MgO-saturated spinel; therefore, the inclusions were saturated with MgO prior to the immersion of the Al_2O_3 rod. As the immersion time was extended, the Mg content of the steel melt decreased gradually, and the MgO content of the inclusions also decreased but remained in the MgO-saturated spinel region. This was because the supply rate of the Mg from the slag was insufficient to compensate for the Mg consumption due to the

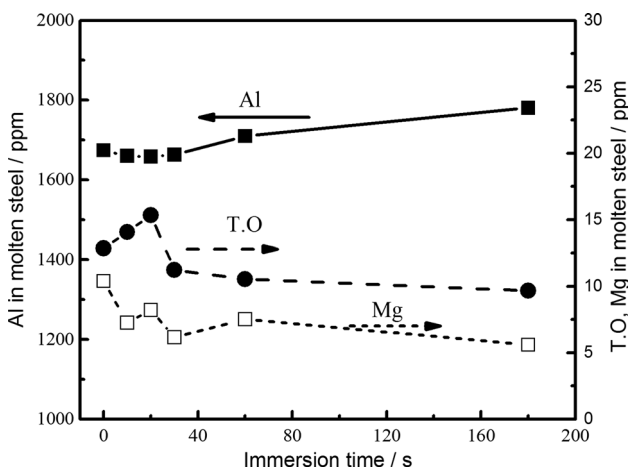
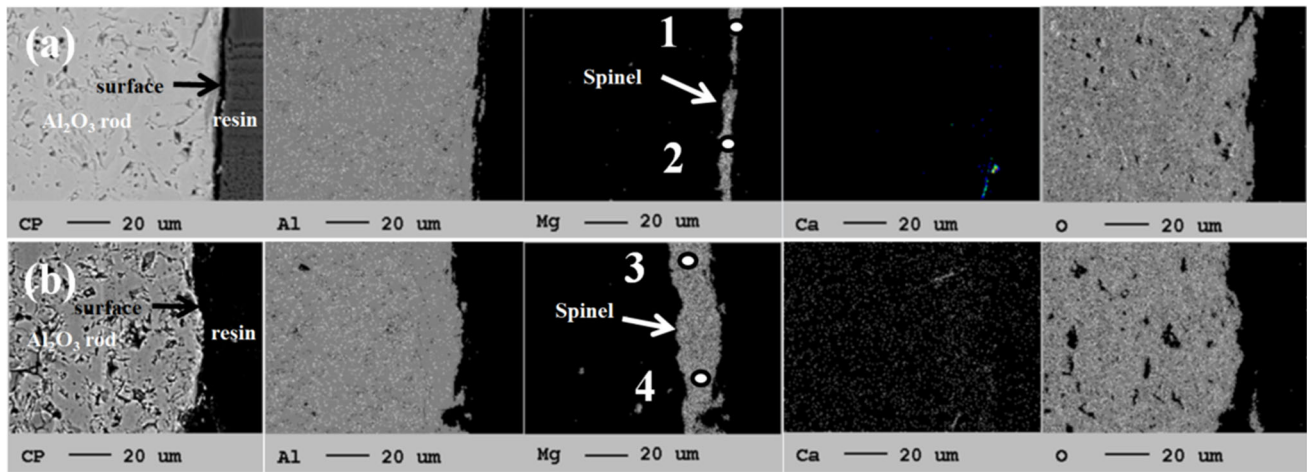


Fig. 3—Variation in the composition of molten steel with immersion time.



position	MgO / %	Al ₂ O ₃ / %	MgO / Al ₂ O ₃
1	18.5	81.5	0.227
2	17.7	82.3	0.215
3	23.6	76.4	0.309
4	22.3	77.7	0.287

Fig. 4—Element mapping of the formed spinel at the Al₂O₃-alloy interface; (a) 10 s immersion period (b) 60 s immersion period.

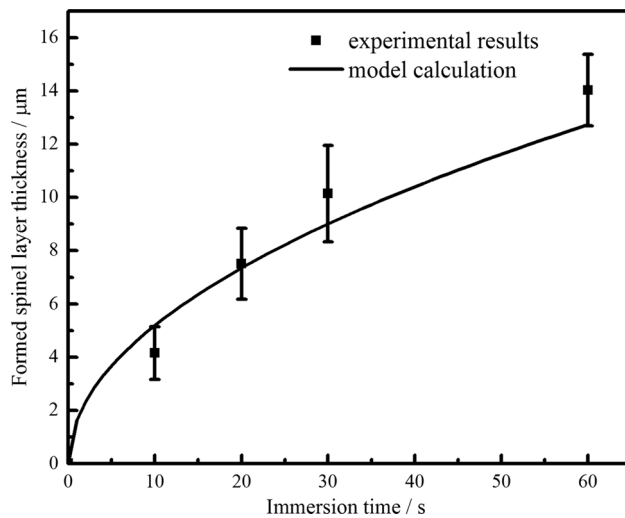


Fig. 5—Variation in the thickness of the formed spinel layer with immersion time.

formation of the spinel layer on the Al₂O₃ rod. In this study, the observed inclusions were smaller than 5 μm.

B. Transformation of Al₂O₃ to Spinel at Various Temperatures

The compositions of the molten steel, following the immersion of the Al₂O₃ rod for 10 and 20 seconds at various temperatures, are shown in Figure 9. The variations in the Mg, Al, and T.O contents with the experimental temperature are negligible. The spinel layer thickness increased with both temperature and the

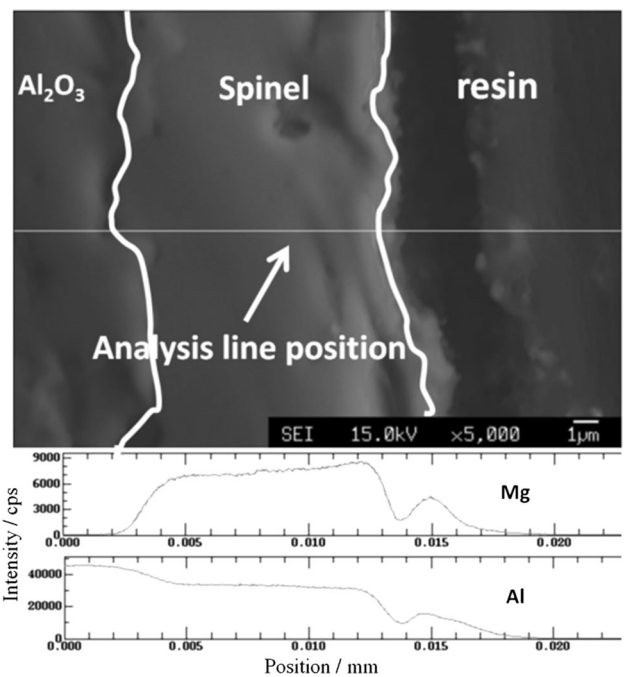


Fig. 6—Concentration gradients of Al and Mg within the formed spinel layer.

immersion time as shown in Figure 10. Both the composition and the elemental gradient of the spinel layers generated at various temperatures were almost the same as those of the spinel layer formed at 1873 K (1600 °C). Although the composition range of spinel changes with temperature, its difference is not so large. For

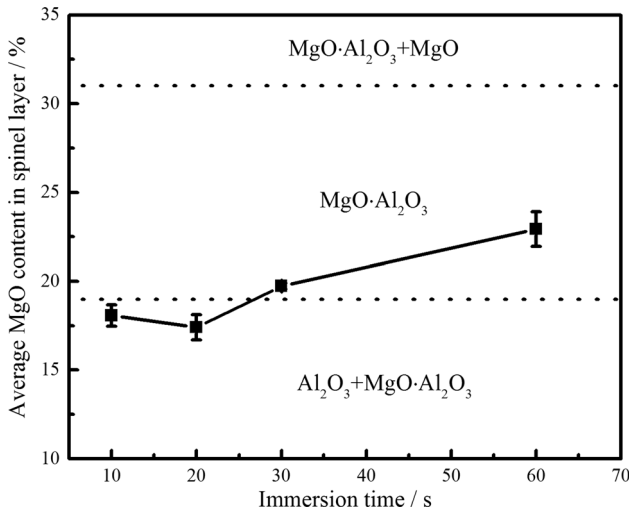


Fig. 7—Variation in the average MgO concentration of the formed spinel layer with immersion time.

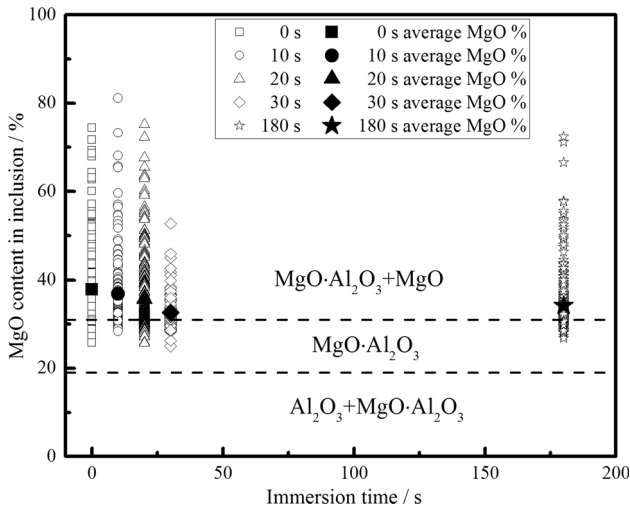


Fig. 8—Variation in the MgO content of the inclusions with immersion time.

example, the concentration range of MgO in spinel is 21 to 28 pct at 1823 K and 18 to 30 pct at 1923 K. Therefore, the clear difference with temperature was not found in this experiment.

IV. DISCUSSION

In this study, a spinel layer with a thickness of 4 μm generated rapidly on the surface of the Al_2O_3 rod within just 10 seconds, following its immersion at 1873 K (1600 $^\circ\text{C}$). To determine the rate-controlling step for the Al_2O_3 transformation, the spinel generation process was considered, as shown in Figure 11. The possible rate-controlling steps of this transformation include (a) Mg transfer at the boundary layer of the molten steel; (b) MgO transfer in the formed spinel layer; and (c) chemical reaction at the formed spinel– Al_2O_3 rod interface. Recently, Sarkar et. al.^[27] proposed a kinetic

model for the dissolution of solid lime in slag, and they considered a similar dissolution process, which is shown in Figure 11. Although the system in the current study is completely different from that in theirs, the kinetic model developed by them can be applied in this study. In this research, the rate of the chemical reaction at 1873 K (1600 $^\circ\text{C}$) was assumed to be sufficiently high, and only the diffusion was considered as the rate-controlling step for this transformation.

By treating the Al_2O_3 rod as a plate with one dimension, and only considering the diffusion of Mg or MgO, the following kinetic equations can be determined for each condition.

A. Mg Diffusion Control in the Boundary Layer of the Molten Steel

The diffusion of the Mg through the boundary layer can be expressed as

$$\frac{d}{dy} (N_{\text{Mg}(-y)}) = 0, \quad [5]$$

where $N_{\text{Mg}(-y)}$ is the combined molar flux of Mg ($\text{mol}/\text{m}^2\text{s}$) and y is the direction.

By integrating Eq. [5] with the boundary conditions listed in Eq. [6], we obtained the growth rate of the spinel layer, based on the assumption of controlled diffusion in the boundary layer of the molten steel, as described in Eq. [7].

$$C_{\text{Mg}} = C_{\text{Mg}}^i \text{ at } y = y_{\text{Al}_2\text{O}_3}^0$$

$$C_{\text{Mg}} = C_{\text{Mg}}^b \text{ at } y = y_{\text{Al}_2\text{O}_3}^0 + \delta_C \quad [6]$$

$$X = \frac{\rho_m D_m}{\rho_{\text{Al}_2\text{O}_3} \delta_C y_{\text{Al}_2\text{O}_3}^0} \ln \left(\frac{\rho_m - C_{\text{Mg}}^i}{\rho_m - C_{\text{Mg}}^b} \right) t, \quad [7]$$

where C_{Mg}^i and C_{Mg}^b are the molar concentration of Mg at the formed spinel–molten steel interface (mol/m^3) and the molar concentration of Mg in the bulk molten steel (mol/m^3), respectively; $y_{\text{Al}_2\text{O}_3}^0$ and δ_C are the initial thickness of the Al_2O_3 plate (m) and the thickness of the boundary layer in the molten steel (m), respectively; t is the reaction time (seconds); ρ_m and $\rho_{\text{Al}_2\text{O}_3}$ are the molar densities of the molten steel (mol/m^3) and Al_2O_3 plate (mol/m^3), respectively; D_m is the Mg diffusion rate in the molten steel (m^2/s), and X is the ratio of the formed product thickness to the initial thickness of the Al_2O_3 plate.

On the right-hand side of expression [7], all the variables can be treated as constants, with the exception of D_m , therefore, expression [7] can be simplified as

$$X = B_1 D_m t, \quad [8]$$

where B_1 indicates $\frac{\rho_m}{\rho_{\text{Al}_2\text{O}_3} \delta_C y_{\text{Al}_2\text{O}_3}^0} \ln \left(\frac{\rho_m - C_{\text{Mg}}^i}{\rho_m - C_{\text{Mg}}^b} \right)$ in Eq. [7] and is a constant independent of temperature.

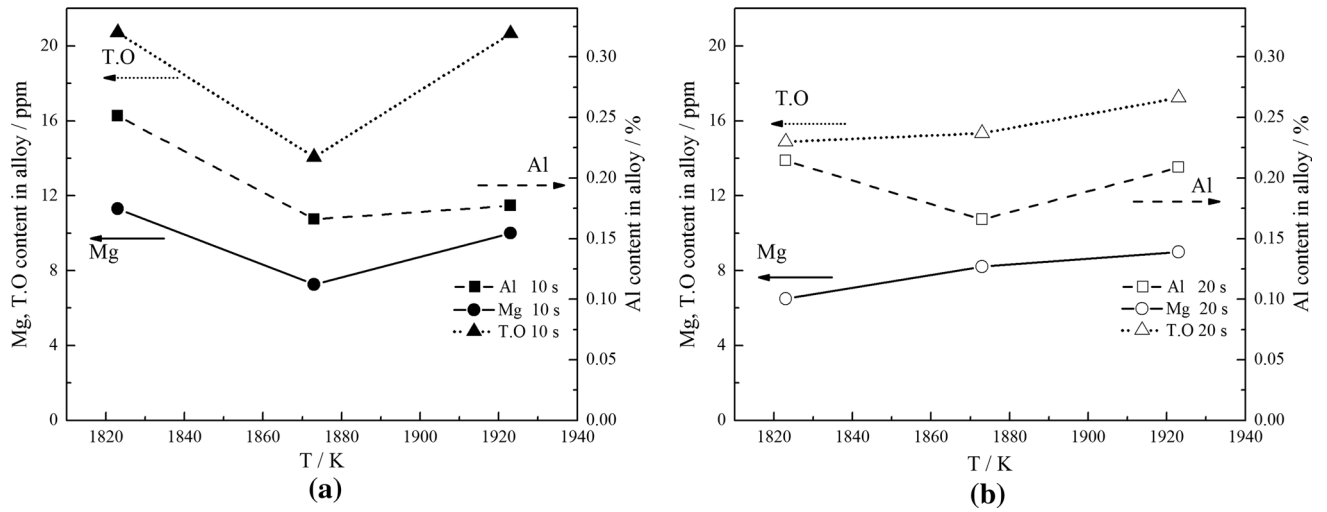


Fig. 9—Variation in the composition of the molten steel with immersion time, under various temperatures; (a) 10 s and (b) 20 s.

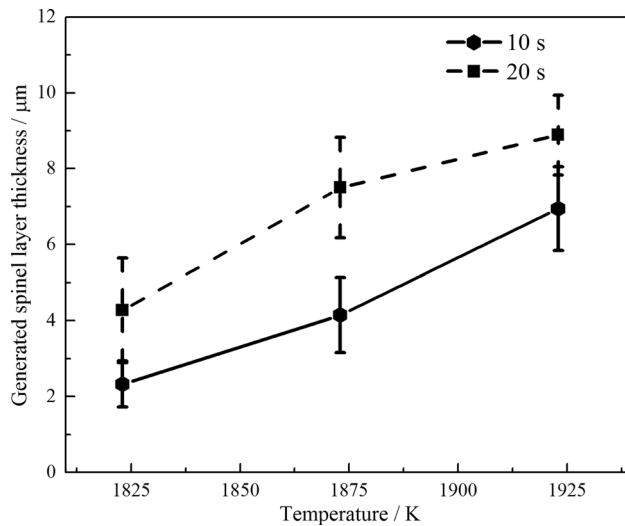


Fig. 10—Variation in the thickness of the formed spinel product under various temperatures.

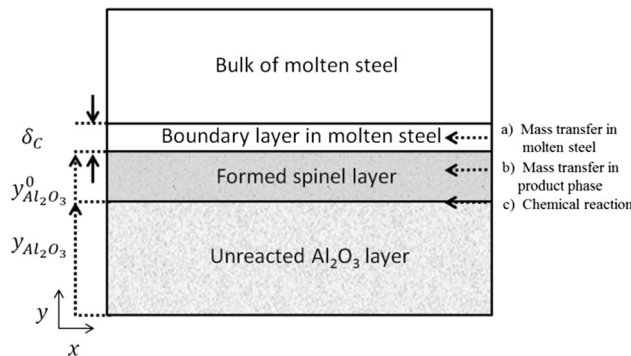


Fig. 11—Illustration of the formation of spinel layer on Al_2O_3 surface.

B. MgO Diffusion Control in Formed Spinel Layer

If the diffusion that occurs in the formed spinel layer functions as the rate-controlling step, the reaction rate could be expressed in a similar manner to Eq. [5]; however, in this case, the boundary conditions differ to those in Eq. [6]. They are listed as follows:

$$C_{\text{MgO}} = C_{\text{MgO}}^i \text{ at } y = y_{\text{Al}_2\text{O}_3}$$

$$C_{\text{MgO}} = C_{\text{MgO}}^s \text{ at } y = y_{\text{Al}_2\text{O}_3}^0, \quad [9]$$

where C_{MgO}^i is the molar concentration of MgO at the interface between the formed spinel layer and unreacted Al_2O_3 surface (mol/m^3); C_{MgO}^s is the molar concentration of MgO at the interface between the formed spinel layer and molten steel (mol/m^3); and $y_{\text{Al}_2\text{O}_3}$ is the thickness of the unreacted Al_2O_3 layer.

By integrating Eq. [5] with the boundary conditions listed in Eq. [9], we obtained the growth rate of the spinel layer by assuming that the MgO diffusion in the formed spinel layer functioned as the rate-controlling step, as described in Eq. [10].

$$X^2 = \frac{D_p}{y_{\text{Al}_2\text{O}_3}^{20}} \ln \left(\frac{\rho_{\text{Al}_2\text{O}_3} - C_{\text{MgO}}^i}{\rho_{\text{Al}_2\text{O}_3} - C_{\text{MgO}}^s} \right) t, \quad [10]$$

where D_p is the Mg diffusion rate in the solid spinel (m^2/s).

On the right-hand side of expression [10], all the variables can be treated as constants, with the exception of D_p ; therefore, expression [10] can be simplified as

$$X^2 = B_2 D_p t, \quad [11]$$

where B_2 indicates $\frac{1}{y_{\text{Al}_2\text{O}_3}^{20}} \ln \left(\frac{\rho_{\text{Al}_2\text{O}_3} - C_{\text{MgO}}^i}{\rho_{\text{Al}_2\text{O}_3} - C_{\text{MgO}}^s} \right)$ in Eq. [11], and it is a constant that is independent of temperature.

To evaluate the rate-controlling step, the activation energy was estimated using the experimental results.

Initially, the values of $B_1 D_m$ and $B_2 D_p$ at each temperature were obtained by the relationship between X or X^2 and t . Subsequently, the activation energy was calculated using the relationship between $B_1 D_m$ or $B_2 D_p$ and the temperature, as shown in Figure 12.

If the Mg diffusion in the boundary layer of the molten steel is assumed to be the rate-controlling step, the evaluated activation energy can be determined to be 240 kJ/mol. However, if the diffusion of the MgO in the formed spinel is assumed to be the rate-controlling step, the activation energy can be determined to be 464 kJ/mol. B_1 and B_2 are independent of temperature; therefore, the obtained activation energy values can be compared with reported values for the activation energy of diffusion. Although the activation energy for the diffusion of Mg in molten steel has not been measured, the diffusion coefficients, and their temperature dependencies, of the various elements in the molten steel do not exhibit large differences.^[28] The measured activation energies of the various elements in the molten steel^[29] are far lower than 240 kJ/mol, which was the value determined in this study. In contrast, the activation energy of the MgO diffusion in the spinel was high. Seetharaman *et al.* investigated the inter-diffusion of Mg and Al in spinel using the diffusion couple method, and they obtained an activation energy of 539.8 kJ/mol over a temperature range of 1473 K to 1873 K (1200 °C to 1600 °C).^[30] Van Orman *et al.* summarized experimental data for cation diffusion in spinel, and showed that the activation energy for Mg-Al inter-diffusion in the spinel was 230 kJ/mol over the temperature range of 833 K to 1873 K (560 °C to 1600 °C).^[31] This value was not directly obtained for Mg-Al inter-diffusion but for Mg-Al cation ordering in spinel; the activation energies for these two processes are similar. The estimated activation energy obtained in this study (464 kJ/mol) was within the range of values published for MgO diffusion in spinel (230 and 539.8 kJ/mol). Assuming that the chemical reaction rate is sufficiently high, based on the similarity between the activation energies, it can

be concluded that the diffusion of MgO in the generated spinel layer functions as the rate-controlling step. In addition, in Figure 6, the Mg and Al concentration gradients observed in the formed spinel layer also support the idea that the MgO diffusion in spinel plays a substantial role with respect to the spinel formation kinetics.

Recently, Galindo *et al.*^[32] developed a kinetic model of the Al_2O_3 -to-spinel transformation. In their model, the mass transfer at the boundary layer of the molten steel and the cationic diffusion at the formed spinel layer are considered. The diffusion in the formed spinel layer was calculated using the Wagner-Schmalzried theory,^[33,34] and the mass transfer rate in the molten steel was estimated using experimental data for the measured reaction rate between the molten slag and steel. The authors concluded that the mass transfer in molten steel was the rate-controlling step for the Al_2O_3 inclusion transformation. To validate this conclusion, precise evaluation of the mass transfer coefficient in molten steel should be studied in future.

After determining the rate-controlling step for the Al_2O_3 transformation, the MgO diffusion coefficient (D_p) of the spinel layer can be obtained using Eq. [10]. For C_{MgO}^i and C_{MgO}^s , MgO concentrations of Al_2O_3 -saturated spinel and MgO-saturated spinel were used based on the phase diagram of Al_2O_3 -MgO system.^[26] The mass percent was converted to mole fraction assuming that the density of spinel was 3.58 g/cm^3 .^[35]

The values of all the parameters used to estimate D_p are listed in Table I, and estimated values of D_p are listed in Table II. The value of composition range of spinel at different temperatures was used for the calculation of D_p at different temperatures. Galindo *et al.*^[32] summarized and compared reported self-diffusion and inter-diffusion coefficients of spinel; the reported values range from $1E-12 \text{ m}^2/\text{s}$ to $1E-18 \text{ m}^2/\text{s}$ at 1873 K (1600 °C), which are close to the estimated value obtained in this study.

The transformation rate of the Al_2O_3 inclusions at 1873 K (1600 °C) was estimated; it was assumed that the inclusions possessed a spherical shape or plate shape. In the case of the spherical phase, the rate of the Al_2O_3 -to-spinel transformation can be calculated using Eq. [12].^[27] In the case of the plate shape, the rate was calculated based on Eq. [10].

$$1 - \frac{2}{3}X - (1 - X)^{2/3} = \frac{D_p}{y_{Al_2O_3}^0} \ln \left(\frac{\rho_{Al_2O_3} - C_{MgO}^i}{\rho_{Al_2O_3} - C_{MgO}^s} \right) t. \quad [12]$$

The calculated transformation rates for Al_2O_3 inclusions with various sizes at 1873 K are shown in Figure 13. In Figure 13, the initial plate thickness is the length of the shortest edge of the plate-shaped inclusion. The calculated transformation rates for Al_2O_3 inclusions with 5 μm in radius (spherical shape) at different temperatures are shown in Figure 14. The time required for the Al_2O_3 inclusion to completely transform increased with the inclusion diameter; it took just 3 seconds for a typical Al_2O_3 inclusion (5 μm in radius,

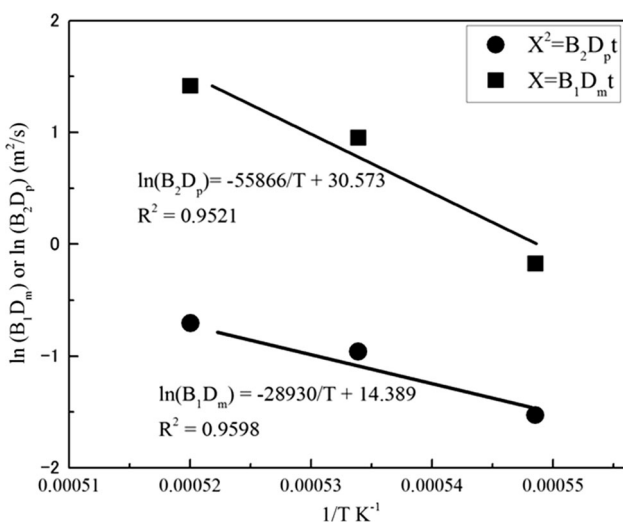


Fig. 12—Temperature dependence of parameters $B_1 D_m$ and $B_2 D_p$, used to estimate the activation energy.

Table I. Parameters Used to Determine the Diffusion Coefficient of MgO in the Spinel

ρ_s (mol m ⁻³)	$\rho_{Al_2O_3}$ (mol m ⁻³)	$y_{Al_2O_3}^0$ (m)
25211	38235	0.003
	C_{MgO}^s (mol m ⁻³)	C_{MgO}^i (mol m ⁻³)
1823 K	25060	18795
1873 K	25955	17005
1923 K	26850	16110

Table II. Estimated Diffusion Coefficient of MgO in the Spinel at Various Temperatures

Temperature	1823 K (1550 °C)	1873 (1600 °C)	1923 (1650 °C)
D_p (m ² s ⁻¹)	2.08E-12	4.93E-12	6.77E-12

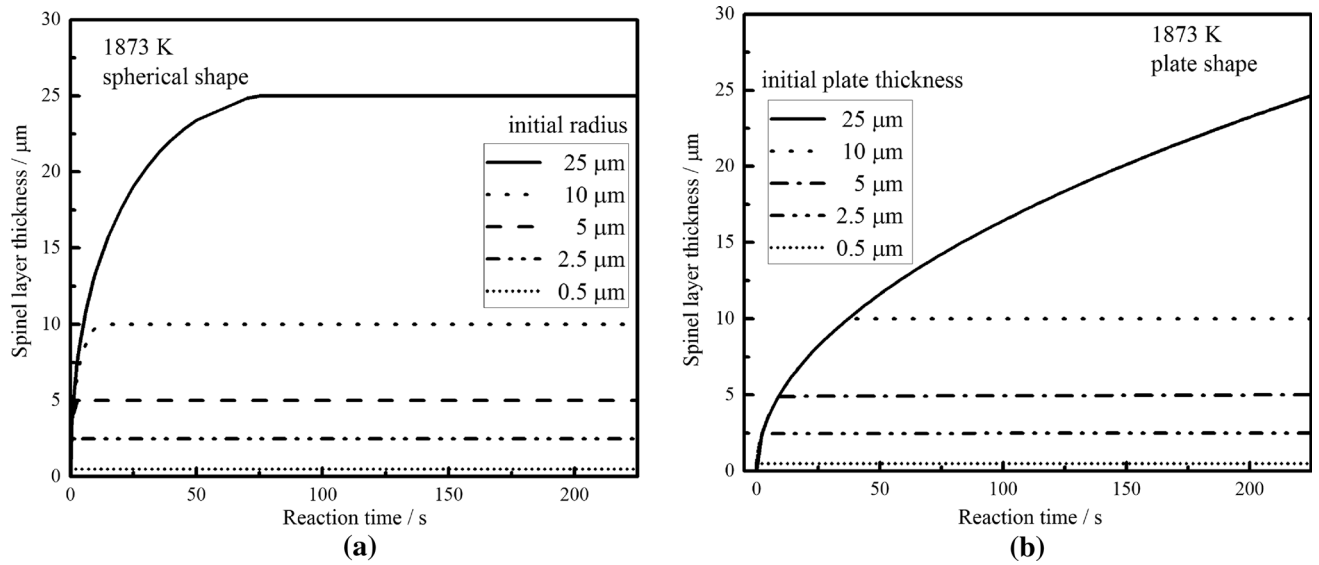


Fig. 13—Estimated transformation rate of Al₂O₃ inclusions with various sizes a) spherical shape b) plate shape.

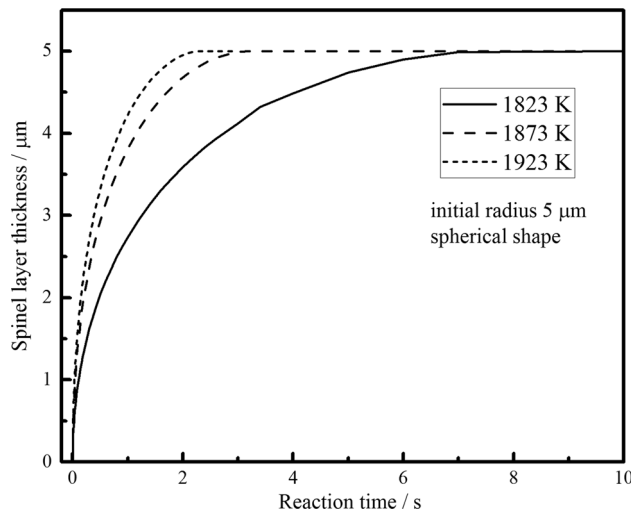


Fig. 14—Estimated transformation rate of Al₂O₃ inclusions with 5 μm in radius of spherical shape at different temperatures.

spherical shape) to transform at 1873 K. In addition, the times for the same transform at 1823 K and 1873 K are 7 and 2.2 seconds, respectively. The transformation rate of the spherically shaped inclusion was greater than that of the plate-shaped inclusion. This is because the spherically shaped inclusion had two dimensions while the plate-shaped Al₂O₃ inclusion was treated as having one dimension with regard to MgO diffusion. By this research, it was found that the transformation rate of Al₂O₃ to spinel is very fast. This indicates that the transfer rate is controlled by the dissolution rate of Mg from slag or refractory. Therefore, to suppress the spinel inclusion formation, it is essential to decrease the dissolution rate of Mg.

V. CONCLUSIONS

In this study, an Al₂O₃ rod was immersed into Mg-containing molten steel to investigate the transformation rate of Al₂O₃ to MgO·Al₂O₃. The following results were obtained:

- (1) The rate of the Al_2O_3 -to- $\text{MgO}\cdot\text{Al}_2\text{O}_3$ spinel transformation was rapid when there was sufficient Mg in the molten steel. Following the immersion, a spinel layer with a thickness of $4\ \mu\text{m}$ formed on the Al_2O_3 rod surface within 10 seconds.
- (2) By evaluating the apparent activation energy, in this research, the rate-controlling step was determined to be the MgO diffusion in the formed spinel layer. The activation energy of the MgO diffusion in the spinel was determined to be 464 kJ/mol.
- (3) Based on the determined rate-controlling step, the diffusion coefficient of the MgO in the $\text{MgO}\cdot\text{Al}_2\text{O}_3$ spinel was calculated. Its value varied from $2.08\text{E}-12\ \text{m}^2/\text{s}$ to $6.77\text{E}-12\ \text{m}^2/\text{s}$ over the temperature range of 1823 K to 1923 K (1550 °C to 1650 °C).

ACKNOWLEDGMENTS

The authors thank Professor Xinhua Wang of Shougang Corporation (earlier at University of Science and Technology, Beijing) for his kind support with regard to the P-SEM analysis. The authors gratefully acknowledge the financial support provided by ISIJ research promotion grant from the Iron & Steel Institute of Japan (ISIJ).

REFERENCES

1. J.-H. Park: *Metall. Mater. Trans. B*, 2007, vol. 38B, pp. 657–63.
2. J.-H. Son, I.-H. Jung, S.-M. Jung, H. Gaye, and H.-G. Lee: *ISIJ Int.*, 2008, vol. 48, pp. 1542–51.
3. A. Harada, G. Miyano, N. Maruoka, H. Shibata, and S.-Y. Kitamura: *ISIJ Int.*, 2014, vol. 54, pp. 2230–38.
4. C. Liu, F. Huang, J. Suo, and X. Wang: *Metall. Mater. Trans. B*, 2016, vol. 47B, pp. 989–98.
5. X. Wang, X. Li, Q. Li, F. Huang, H. Li, and J. Yang: *Steel Res. Int.*, 2014, vol. 85, pp. 155–63.
6. G. Okuyama, K. Yamaguchi, S. Takeuchi, and K. Sorimachi: *ISIJ Int.*, 2000, vol. 40, pp. 121–28.
7. C. Liu, F. Huang, and X. Wang: *Metall. Mater. Trans. B*, 2016, vol. 47B, pp. 999–1009.
8. K. Fujii, T. Nagasaka, and M. Hino: *ISIJ Int.*, 2000, vol. 40, pp. 1059–66.
9. J.-H. Park and H. Todoroki: *ISIJ Int.*, 2010, vol. 48, pp. 1333–46.
10. M. Jiang, X. Wang, B. Chen, and W. Wang: *ISIJ Int.*, 2010, vol. 48, pp. 95–104.
11. W.-Y. Cha, D.-S. Kim, Y.-D. Lee, J.-J. Park: *ISIJ Int.*, 2004, vol. 44, pp. 1134–39.
12. T. Yoshioka, K. Nakahata, T. Kawamura, and Y. Ohba: *ISIJ Int.*, 2016, vol. 56, pp. 1973–81.
13. E. Sunami, S. Nozaki, Y. Miura, and T. Miura: *Tetsu-to-Hagané*, 1982, vol. 68, p. S248.
14. O. Suzuki, M. Ogchi, K. Nohara, T. Emi, Y. Mihara, and Y. Katayama: *Tetsu-to-Hagané*, 1982, vol. 68, p. S249.
15. R. Nakao, H. Tsuboi, E. Takeuchi, H. Morishige, and M. Miyake: *Tetsu-to-Hagané*, 1987, vol. 73, p. S941.
16. H. Matsuno and Y. Kikuchi: *Tetsu-to-Hagané*, 2002, vol. 88, pp. 48–50.
17. Y. Ehara, S. Yokoyama, and M. Kawakami: *Tetsu-to-Hagané*, 2007, vol. 93, pp. 475–82.
18. Y. Ehara, S. Yokohama, and M. Kawakami: *Tetsu-to-Hagané*, 2007, vol. 93, pp. 208–14.
19. Y. Kang, B. Sahebkar, P.R. Scheller, K. Morita, S. Du: *Metall. Mater. Trans. B*, 2011, vol. 42B, pp. 522–34.
20. J.H. Park, S.B. Lee, and H.R. Gaye: *Metall. Mater. Trans. B*, 2008, vol. 39B, pp. 853–61.
21. C.W. Seo, S.H. Kim, S.K. Jo, M.O. Suk, and S.M. Byun: *Metall. Mater. Trans. B*, 2010, vol. 41B, pp. 790–97.
22. J.H. Park: *Metall. Mater. Trans. B*, 2007, vol. 38B, pp. 657–63.
23. J.H. Park: *Metall. Mater. Trans. B*, 2005, vol. 36B, pp. 495–502.
24. S.K. Jo, B. Song, and S.H. Kim: *Metall. Mater. Trans. B*, 2002, vol. 41B, pp. 703–09.
25. H. Itoh, M. Hino, and S. Ban-Ya: *Metall. Mater. Trans. B*, 1997, vol. 28B, pp. 953–56.
26. Slag Atlas, 2nd ed., Verein Deutscher Eisenhüttenleute, pp. 44–44.
27. R. Sarkar, U. Roy, and D. Ghosh: *Metall. Mater. Trans. B*, 2016, vol. 47B, pp. 2651–65.
28. K. Nagata, N. Sata, and K. Goto, *Tetsu-to-Hagané*, 1982, vol. 68, pp. 1694–705.
29. Y. Ono: *Tetsu-to-Hagané*, 1977, vol. 63, pp. 1350–61.
30. P. Zhang, T. Debroy, and S. Seetharaman: *Metall. Mater. Trans. A*, 1996, vol. 27A, pp. 2105–14.
31. J.A. Van Orman and K.L. Crispin: *Reviews in Mineralogy & Geochemistry*, 2010, vol. 72, pp. 757–825.
32. A. Galindo: Master's thesis, McMaster University, 2015. <https://macsphere.mcmaster.ca/handle/11375/18449>.
33. C. Wagner: *Prog. Solid State Chem.*, 1975, vol. 10, pp. 3–16.
34. T. Pfeiffer and H. Schmalzried: *Zeitschrift Für Physikalische Chemie*, 1989, vol. 161, pp. 1–17.
35. I. Ganesh: *Int. Mater. Rev.*, 2013, vol. 58, pp. 63–112.